Manganese Incorporation into the Mesoporous Material MCM-41 under Acidic Conditions as Studied by High Field Pulsed EPR and ENDOR Spectroscopies

Jingyan Zhang and Daniella Goldfarb*

Contribution from the Department of Chemical Physics, Weizmann Institute of Science, Rehovot 76100, Israel

Received November 29, 1999. Revised Manuscript Received May 12, 2000

Abstract: The incorporation of Mn(II) into the mesoporous material MCM-41, synthesized under acidic conditions with $[Si]/[H^+]$ in the range of 0.1−0.4 was investigated. Tetraethyl-orthosilicon (TEOS) was used as the silica source and cetyltrimethylammonium chloride or bromide (CTAC/CTAB) as the structure-directing agent. The Mn(II) sites in the final product were characterized by high-field (W-band, 95 GHz) pulsed EPR and electron−nuclear double resonance (ENDOR) spectroscopies that provided highly resolved EPR spectra and detailed information concerning the Mn(II) coordination sphere. These measurements were complemented with X-band continuous wave (CW) EPR and electron-spin−echo envelope modulation (ESEEM) spectroscopies. In addition, the bulk properties of the final products were characterized by X-ray diffraction and ^{29}Si MAS NMR, while in situ X-band CW EPR measurements on reaction mixtures containing the spin probe 5-doxyl stearic acid (5DSA) were carried out to follow the reaction kinetics and the degree of silica condensation. These bulk properties were then correlated with the formation of the different Mn(II) sites. The final product consists of a mixture of two hexagonal phases (d = 38, 43 Å), the relative amounts of which depend on the $[Si]/[H^+]$ in the starting gel. Two Mn(II) sites, which exhibit unresolved overlapping signal in the X-band EPR spectra, were easily distinguished in the low-temperature field-sweep (FS) echo-detected (ED) W-band spectra due to their significantly different ^{55}Mn hyperfine couplings. One Mn(II) site, *a*, is characterized by a hyperfine splitting of 97 G, and the second, *b*, by 82 G. The relative amount of *b* increases with increased acidity. Site *a* is assigned to a hexa-coordinated Mn(II) with water ligands that is anchored to the internal pore surface of the silica either by one coordination site or through hydrogen bond(s). The Mn(II) in site *b* is in a distorted tetrahedral coordination, located within the first few layers of the silica wall. When the water content of the final products increases, site *b* assumes characteristics that are very similar to site *a*, suggesting that the silica wall is "soft" and not fully condensed. The NMR and in situ EPR measurements show that incomplete TEOS hydrolysis and slow silica polymerization, which occurs for $[Si]/[H^+] > 0.1$, favors the formation of site *a*, whereas complete hydrolysis and fast polymerization, generating enough acidic Si−OH groups, favors the formation of site *b*. The incomplete hydrolysis also accounts for the generation of two hexagonal phases.

Introduction

The M41S mesoporous materials[1] have drawn considerable attention due to their unique physical properties, namely large pore size, narrow pore size distribution, high specific surface area, and long-range ordering of the pore packing, which are important for potential applications in the field of catalysis. This has stimulated rapid developments in synthetic routes producing new mesostructural materials, and in surface modification of the final products. The most extensively studied member of the mesoporous materials family has been MCM-41, which exhibits an hexagonal array of pores. In terms of catalytic activity, however, MCM-41 is not as active in processing bulky molecules as desired.[2] Consequently, many studies have focused on the introduction of catalytically active species into silicious MCM-41.[1,3,4] Two general approaches were employed: in the first, the active species are incorporated into the silica during the synthesis,[3,4] whereas in the second, functional groups are anchored to the silica surface after synthesis.[5,6]

Incorporation of transition metal ions is a common method for introducing active sites in zeolites and zeotype materials.[7] There are numerous reports of doping MCM-41 with a variety of metal elements, including Al, Ti, Fe, Mn, B, Zr, Cr, Ga, V, Sn, Co, and Nb, as recently reviewed by Ying et al.[8] In many applications the metal-containing MCM-41 materials have been found to be better acid catalysts than the original silicious MCM-41.[9−11] Doped MCM-41 materials are usually prepared by

(1) Beck, J. S.; Vartuli, J. C.; Roth, W. J.; Leonowicz, M. E.; Kresge, C. T.; Schmidt, K. D.; Chu, C. T.-W.; Olson, D. H.; Shepard, E. W.; McCullen, S. B.; Higgins, J. B.; Schlenker, J. L. *J. Am. Chem. Soc.* **1992**, *114*, 10834−10843.

(2) Corma, A.; Grand, M. S.; Gonzalez-Alfrao, V.; Orichilles, A. V. *J. Catal.* **1996**, *159*, 375−382.

(3) Corma, A.; Camblor, M. A.; Esteve, P.; Martínez, A.; Pérez-Pariente, J. *J. Catal.* **1994**, *151*, 151−158.

(4) Reddy, K. M.; Mondrakovski, I.; Sayari, A. *J. Chem. Soc., Chem. Commun.* **1994**, 1059−1060.

(5) Moller, K.; Bein, T. *Chem. Mater.* **1998**, *10*, 2950−2963.

(6) Luan, Z.; Xu, J.; Kevan, L. *Chem. Mater.* **1998**, *10*, 3699−3706.

(7) Szostak, R. *Molecular sieves Principles of Synthesis and Identification*; Van Nostrand Reinhold: New York, 1989; pp 211−238.

(8) Ying, Y. J.; Mehnert, C. P.; Wong, M. S. *Angew. Chem., Int. Ed.* **1999**, *38*, 56−77.

(9) Zhao, X. S.; Lu, G. Q.; Millar, G. *Int. Eng. Chem. Res.* **1996**, *35*, 2075−2090.

10.1021/ja994165n CCC: $19.00
Published on Web 07/06/2000

adding the metal salts to the reaction mixture under basic conditions,[12,13] although several preparations under acidic conditions were reported as well.[12,14] The successful incorporation of the metal elements into the silica is, however, not predictable and is highly dependent on the preparation method and the pH of the synthesis mixture. Moreover, the incorporated metal ions often leach from the silica during calcination.[8] These shortcomings led to the design of post-synthesis metal incorporation methods.[15,16] There, the metal ions are grafted onto the siliceous wall after synthesis using various nonaqueous solutions of metal salts. In addition, a template-ion exchange method has been proposed where the template ions in the final product are exchanged for metal ions in aqueous solution.[17]

The different approaches for metal ion incorporation mentioned above were employed to introduce Mn(II) into MCM-41,[12−14,16,17] and its location was explored primarily by EPR spectroscopy and/or by comparison of the ion exchange capacity and catalytic activity with those of silicious MCM-41.[12,14] Most of these studies, however, are ambiguous in terms of the Mn(II) location and coordination state.[13] The majority of the EPR measurements on Mn(II) in MCM-41 have been carried out at conventional X-band (∼9.5 GHz) frequencies and a few at Q-band (∼35 GHz) frequencies.[13,14] The X-band spectra often suffer from low resolution, preventing the detection of Mn(II) centers with different hyperfine couplings, which are characteristic of the metal oxidation and coordination state. Consequently, the local environment of the Mn(II) is not well determined and centers with different properties cannot be distinguished.

The recent developments of high-field EPR ($\upsilon > 75$ GHz, $B_0 > 2.5$ T)[18] and electron−nuclear double resonance (ENDOR) spectroscopies[19,20] offer new opportunities for high-spin systems such as Mn(II) ($S = {}^5/_2$, $I = {}^5/_2$) due to the improved spectral resolution in orientationally disordered samples.[21,22] This is primarily due to the reduction of the high-order effects of the zero field splitting (ZFS) and the hyperfine interaction on the spectrum. Consequently, the inhomogeneous broadening of the allowed central EPR transitions, $|-{}^1/_2, m\rangle \rightarrow |{}^1/_2, m\rangle$, decrease and the intensity of the forbidden transitions, $|-{}^1/_2, m\rangle \rightarrow |{}^1/_2, m \pm 1\rangle$, is considerably reduced.[23] The higher resolution of the high-field EPR spectrum facilitates significantly ENDOR measurements, which provide details on the coordination sphere of the metal ion.[22]

In this work we explore the synthesis of MnMCM-41 under acidic conditions ($[Si]/[H^+] = 0.1-0.4$) where Mn(II) is not oxidized to Mn(III) during the synthesis.[14] Two groups of techniques were applied; the first includes X-ray diffraction and ^{29}Si MAS NMR used for the characterization of the final products, and in situ X-band EPR measurements of a spin-probe added to the reaction mixture designed to explore the rate of silicate polymerization. The second group consists of methods aimed at the characterization of the Mn(II) sites formed under acidic conditions. These include X-band (9 GHz) continuous wave (CW) EPR and electron-spin−echo envelope modulation (ESEEM) spectroscopies, and high-field (W-band, 95 GHz) EPR and ENDOR measurements. The latter provided unusually resolved EPR spectra that allowed the identification and characterization of two types of Mn(II) centers. One center was assigned to tetrahedrally coordinated Mn(II) located within the silica, though close to the internal pore surface, whereas the other is hexa-coordinated hydrated Mn(II) attached to the internal surface of the silica. The relative amounts of the two Mn(II) centers in samples prepared with different $[Si]/[H^+]$ in the starting gel were then correlated with the bulk properties of the materials, providing insight into the factors that control the incorporation of Mn(II) into the silica network under the conditions used.

Experimental Section

Synthesis. Manganese-containing MCM-41 (MnMCM-41) was synthesized as described previously[14] using tetraethyl-orthosilicon (TEOS, Aldrich 98%) as the silica source and cetyltrimethylammonium chloride (CTAC, 25 wt % aqueous solution, Aldrich) or cetyltrimethylammonium bromide (CTAB, Aldrich) as the structure-directing agent. CTAB deuterated at the α-position was synthesized as described in the literature.[24] In a typical preparation, 6 mL of HCl (2 N, 12 mmol) are combined, under stirring, with 10 mL of an aqueous solution with 0.55 mmol CTAC and 0.56 mmol $MnSO_4$. The mixture is stirred for 10 additional minutes, followed by the addition of 1.02 mL (4.6 mmol) TEOS. The resulting mixture is left under stirring for 24 h at room temperature (298 K). The solid precipitate is recovered by filtration, washed with distilled water several times, and dried in air at an ambient temperature. The molar compositions of the synthesis gels were as follows: TEOS: 0.12CTAC: (2.6−10.4)HCl: 174H_2O: 0.12Mn(II). Chemical analysis showed that for $[Si]/[H^+] = 0.1$ and 0.4 only 4% and 9%, respectively, of the total Mn(II) added to the reaction mixture are incorporated into the final products. Calcination was carried out at 813 K for 1 h in flowing nitrogen, followed by 6 h in flowing air. In some preparations the template was removed by solvent extraction where the as-synthesized MCM-41 sample was mixed with a 1 M HCl solution in ethanol (liquid:solid = 300 mL/g) at 343 K for 30 h.[25]

MnMCM-41 was also prepared by the template-ion exchange method as described by Yonemitsu et al.[17] Mn(II) ion implantation was obtained by stirring as-synthesized hydrothermally stable MCM-41 (0.4 g)[26] in 8 mL of an aqueous solution of manganese acetate (0.04 M) at an ambient temperature for 1 h. The mixture was kept at 353 K in a water bath for 20 h without stirring. The resulting solid was filtered, washed with deionized water, and dried at 353 K for 1 h. Calcination was carried out as described above.

The spin probe 5-doxyl stearic acid (5DSA) was employed in the in situ X-band EPR measurements. The reaction mixture was prepared as described above with the exception that 1.0 mg (2.6×10^{-6} mol) of 5DSA was added to the surfactant solution and the $MnSO_4$ was omitted.

Characterization. X-ray diffraction (XRD) patterns of the products were obtained from thin layers of sample on glass slides and measurements were carried out on a Rigaku D/Max-B diffractometer,

(10) Corma, A.; Martinez, A.; Martinez-Soria, V.; Monton, J. B. *J. Catal.* **1995**, *153*, 25−31.
(11) Blasco, T.; Corma, A.; Navarro, M. T.; Perez-Pariente, J. *J. Catal.* **1995**, *156*, 65−74.
(12) Zhang, W.; Wang, J.; Tanev, P. T.; Pinnavaia, T. J. *J. Chem. Soc., Chem. Commun.* **1996**, 979−980.
(13) Xu, J.; Luan, Z.; Wasowicz, T.; Kevan, L. *Microporous Mesoporous Mater.* **1998**, *22*, 179−191.
(14) Zhao, D.; Goldfarb, D. *J. Chem. Soc., Chem. Commun.* **1995**, 875−876.
(15) Mokaya, R.; Jones, W. *J. Chem. Soc., Chem. Commun.* **1997**, 2185−2186.
(16) Ryoo, R.; Jun, S.; Kim, J. M.; Kim, M. J. *J. Chem. Soc., Chem. Commun.* **1997**, 2225−2226.
(17) Yonemitsu, M.; Tanaka, Y.; Iwamoto, M. *Chem. Mater.* **1997**, *9*, 2679−2681.
(18) Lebedev, Ya. S. *Appl. Magn. Reson.* **1994**, *7*, 339−362.
(19) Disselhorst, J. A. J. M.; Vandermeer, H.; Poluektov, O. G.; Schmidt, J. *J. Magn. Reson.* **1995**, *115*, 183−188
(20) Prisner, T. F.; Rohrer, M.; Möbius, K. *Appl. Magn. Reson.* **1994**, *7*, 167−183.
(21) Bellew, B. F.; Halkides, C. J.; Gerfen, G. J.; Griffin, R. G.; Singel, D. J. *Biochemistry* **1996**, *35*, 12186−12193.
(22) Arieli, D.; Vaughan, D. E. W.; Strohmaier, K. G.; D. Goldfarb D. *J. Am. Chem. Soc.* **1999**, *121*, 6028−6032.
(23) Reed, G. H.; Markham, G. D. *Biological Magnetic Resonance*; Berliner, L., Reuben, J., Eds.; Plenum Press:New York, 1984; Vol. 6, pp 73−142.
(24) Firouzi, A.; Atef, F.; Oertli, A. G.; Stucky, G. D.; Chmelka., B. F. *J. Am. Chem. Soc.* **1997**, *119*, 3596−3610.
(25) Chen, C.; Li, H.; Davis, M. E. *Microporous Mater.* **1993**, *2*, 17−26.
(26) Ryoo, R.; Jun, S. *J. Phys. Chem.* **1997**, *101*, 317−320.

using Cu Kα radiation. Transmission electron microscopy (TEM) images were obtained on a Phillips CM120 transmission electron microscope operating at 120 kV. The samples were prepared by placing a MnMCM-41 powder on Callodion-carbon 400 mesh electron microscope grids from a sonicated 1:1 water−ethanol suspension that was blotted after 30 s. The Si and Mn contents of the final product were determined by inductively coupled plasma atomic emission spectrometry (ICP). The samples (125 mg) were dissolved in concentrated nitric acid and measured versus standards from Merck. Carbon, nitrogen, and hydrogen were analyzed with a Carlo Erba EA-1108 Elemental analyzer.

X-band CW-EPR spectra were recorded using a Varian E−12 spectrometer. Electron-spin−echo envelope modulation measurements (ESEEM) were carried out at 4 K on a home-built X-band pulsed EPR spectrometer[27,28] employing the three-pulse sequence ($\pi/2-\tau-\pi/2-T-\pi/2-\tau-$echo) with the appropriate phase cycling.[29] The pulse length was 0.02 μs and the τ values were selected to optimize the modulation from ^{14}N and ^{2}H nuclei.[30] W-band field-sweep echo-detected (FS-ED) EPR and ENDOR spectra were recorded at 4.5 K on a home-built spectrometer operating at 94.9 GHz.[31] The FS-ED EPR spectra were recorded using the two-pulse echo sequence with microwave (MW) pulse durations of 0.04 and 0.06 μs, respectively, and $\tau = 0.25$ μs. ENDOR spectra were measured using the Davies-ENDOR sequence ($\pi-T-\pi/2-\tau-\pi-\tau-$echo with a radio frequency (RF) π pulse applied during the time interval T). The MW pulse durations were 0.2, 0.1, 0.2 μs, respectively, and the RF pulse length was 19 μs. The magnetic field in the W-band measurements was calibrated using the ^{1}H Larmor frequency determined from the ENDOR experiments.

In situ X-band EPR experiments were done as described elsewhere[32,33] and ^{29}Si MAS NMR spectra were recorded on Bruker CXP 300 MHz spectrometer. Seven millimeter rotors spinning at 3 kHz were employed, and for each spectrum 1200 FID's, obtained after a single $\pi/2$ pulse (3 μs) at intervals of 80 s, were collected.

Results

We first present the results obtained from methods characterizing the bulk properties of the MCM-41 materials obtained with different [Si]/[H$^+$] in the starting gel and then proceed with the characterization methods of the Mn(II) sites.

Characterization of the MCM-41 Products. (a) Powder X-ray Diffraction. The XRD patterns of as-synthesized Mn-MCM-41 materials, prepared with different amounts of HCl, are shown in Figure 1. When [Si]/[H$^+$] = 0.4, the final product is a hexagonal phase with $d = 43$ Å, referred to as phase A. Upon decreasing [Si]/[H$^+$] to 0.21, a new additional hexagonal phase, B, with $d = 38$ Å appeared (Figure 1). A further increase in [H$^+$] causes an increase in the relative amount of phase B, and at [Si]/[H$^+$] = 0.1 the final product contains exclusively phase B. Calcination does not alter significantly the relative amounts of the two phases, although all reflections are shifted to lower angles (see Figure 1). This is consistent with earlier reports of structure contraction upon calcination.[1] The persistence of the ordered structure after calcination supports the assignment of the two phases to hexagonal structures. TEM images (not shown), obtained from samples consisting of either phase A or B, exhibit hexagonal structures with a hole-to-hole distance larger for phase A, consistent with the XRD data.

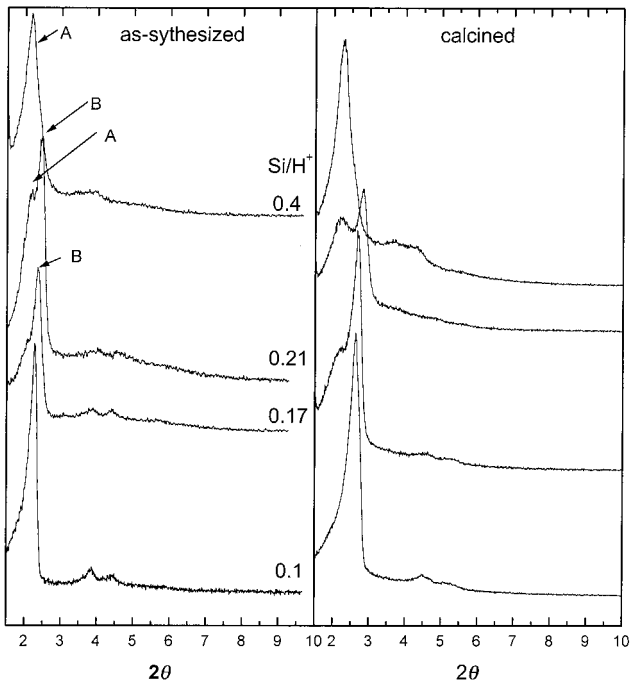

Figure 1. Powder XRD patterns of as-synthesized and calcined MnMCM-41 samples prepared with different [Si]/[H$^+$] ratios as noted on the figure.

(b) ^{29}Si MAS NMR Measurements. The final products were also characterized by ^{29}Si MAS NMR to understand the differences between phases A and B. The spectra of as-synthesized MCM-41 prepared with [Si]/[H$^+$] = 0.4 and 0.1 are shown in Figure 2. The spectrum of the [Si]/[H$^+$] = 0.1 sample exhibits three peaks assigned to Q_2, Q_3, and Q_4, similar to earlier reports.[25] In contrast, the spectrum of as-synthesized MCM-41 prepared with [Si]/[H$^+$] = 0.4 shows in addition to the Q_3 and Q_4 signals (−100 and −110 ppm, respectively) two narrower peaks at −90 and −97 ppm. The latter are attributed to organo-silicon species that are intermediates in the hydrolysis process of TEOS. The 90 ppm signal corresponds to $(EtO)_3Si-O-Si(OEt)_3$,[34] and that at −97 ppm is due to the middle group of linear trisilicic ester $(EtO)_3Si-O-Si(OEt)_2-O-Si(EtO)_3$.[34] The sample prepared with [Si]/[H$^+$] = 0.4 was also measured after calcination and solvent extraction, as shown in Figure 2c,d. The two narrow peaks disappeared after both treatments, and the relative intensity Q_3 and Q_4 has also changed. The calcination process decomposes these species and the further dehydroxylation leads to broadening of the Q_2, Q_3 and Q_4 peaks as reported earlier.[25] Interestingly, the extraction process also causes dehydroxylation, as evident from the increase of Q_4/Q_3 without inducing broadening caused by calcination.

(c) In Situ EPR Measurements. Additional insight into the differences between the materials obtained with different [Si]/[H$^+$] can be obtained by exploring reaction kinetics and the rate of silicate polymerization as obtained from in situ EPR measurements of spin-probes introduced into the reaction mixture.[32,33] Such experiments were carried out for the synthesis with [Si]/[H$^+$] = 0.1 and 0.4 using the spin-probe 5DSA. In these preparations the Mn(II) was not added to avoid overlap with the 5DSA EPR signal. Since the amount of Mn(II) in

(27) Goldfarb, D.; Fauth, J. M.; Tor, Y.; Shanzer, A. *J. Am. Chem. Soc.* **1991**, *113*, 1941−1948.
(28) Shane, J. J.; Gromov, I.; Vega, S.; Goldfarb, D. *Rev. Sci. Instrum.* **1998**, *69*, 3357−3364.
(29) Fauth, J. M.; Schweiger, A.; Braunschweiler, L.; Forrer J.; Ernst, R. R. *J. Magn. Reson.* **1986**, *66*, 74−85.
(30) Kevan, L. *Time Domain Electron Spin Resonance*; Kevan, L., Schwartz, R. N., Eds.; Wiley: New York, 1979; pp 279−341.
(31) Gromov, I.; Krymov, V.; Manikandan, P.; Arieli, D.; Goldfarb, D. *J. Magn. Reson.* **1999**, *139*, 8−17.
(32) Zhang, J.; Luz, Z.; Goldfarb, D. *J. Phys. Chem. B* **1997**, *101*, 7087−7094.
(33) Zhang, J.; Luz, Z.; Goldfarb, D. *J. Phys. Chem. B* **2000**, *104*, 279−285
(34) Pouxviel, J. C.; Boilot, J. P. *J. Noncryst. Solids* **1986**, *89*, 345−360.

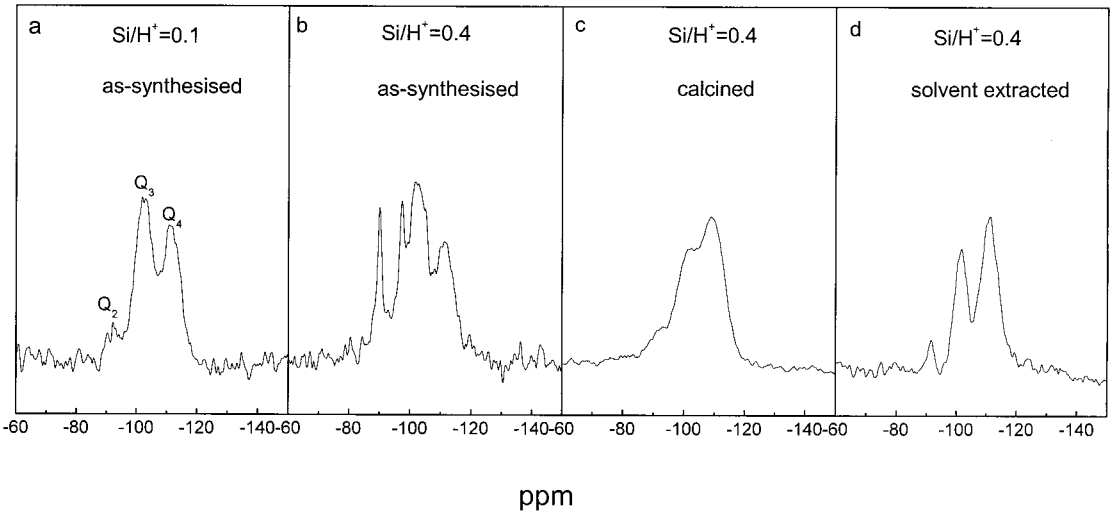

Figure 2. ^{29}Si MAS NMR spectra (298 K) of the as-synthesized MCM-41 prepared with [Si]/[H^+] (a) 0.1, (b) 0.4, (c) same as (b) after calcination, and (d) same as (b) after solvent extraction.

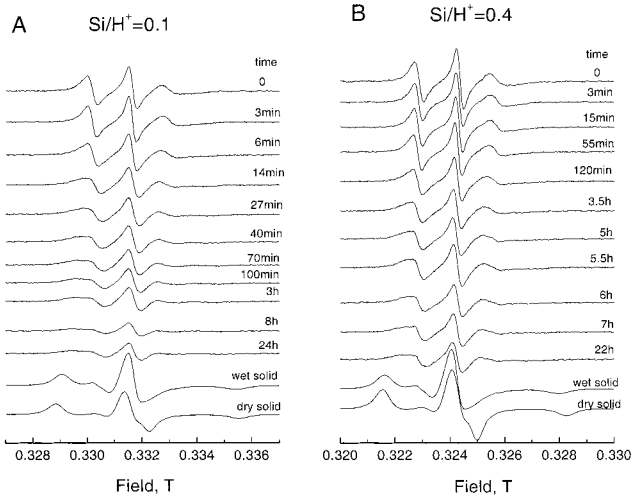

Figure 3. The time evolution of the X-band CW EPR spectrum (recorded at 298 K) of the spin-probe 5DSA during the course of the synthesis of MCM-41 prepared with [Si]/[H^+] = 0.1 (A) and [Si]/[H^+] = 0.4 (B).

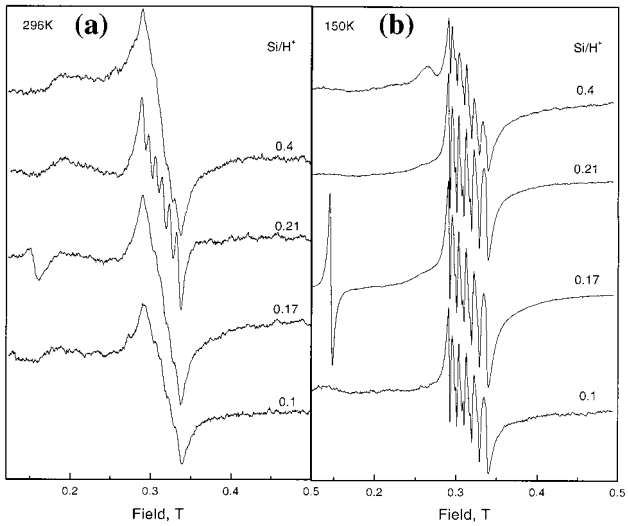

Figure 4. (a) CW X-band EPR spectra of as-synthesized MnMCM-41 prepared with different [Si]/[H^+], recorded at (a) 296 and (b) 150 K (ν = 9.162 GHz).

MnMCM-41 is small, its elimination is not expected to affect the course of the reaction. The nitroxide radical is located near the interface of the organic and inorganic phases, and therefore its motional characteristics are very sensitive to the ordering of the organic phase and to the polymerization of the inorganic phase.[33] The time evolution of the spectrum of 5DSA during the formation of MCM-41 ([Si]/[H^+] = 0.1) is shown in Figure 3A, where the time $t = 0$ corresponds to initiation of the reaction by the addition of TEOS. With time, the spectra exhibit increasing anisotropy, which is characteristic of decreased rotational diffusion rate and increasing order.[33] The spectra recorded after 8 and 24 h are the same, indicating that the process is completed within 8 h. In contrast, the time evolution of the EPR spectrum of 5DSA in the reaction mixture with [Si]/[H^+] = 0.4, shown in Figure 3B, indicates a significantly slower rate of formation. Spectral changes are evident also after 22 h and the line-shape of the 22 h spectrum is similar to the 100 min spectrum of the more acidic gel. This indicates that the silica polymerization, which is the main factor that limits the surfactant mobility, is significantly faster in the [Si]/[H^+] = 0.1 gel mixture. The line-shape of 5DSA in the final product is sensitive to the water content in both samples (see the two lower traces in Figure 3A,B). This suggests that the presence of water "softens" the silica wall, permitting a higher mobility of the surfactant molecules.

Characterization of the Mn(II) Sites. (a) EPR Measurements. The first method employed to characterize the Mn(II) sites was standard X-band CW EPR spectroscopy. The RT X-band EPR spectra of as-synthesized MnMCM-41 prepared with different [Si]/[H^+] are presented in Figure 4a. All spectra show a major signal centered at $g = 2$ with a poorly resolved ^{55}Mn hyperfine splitting assigned to the Mn(II) $|-1/2, m\rangle \rightarrow |1/2, m\rangle$ EPR transitions.[23] This signal is superimposed on a broad signal corresponding to the other EPR transitions. A $g = -4.3$ signal, characteristic of Fe(III) impurities, appeared in some of the samples as well.[35] The spectra recorded at 150 K are better resolved (Figure 4b) and show clear shoulders characteristic of the forbidden transitions. The differences between the room temperature and low-temperature spectra indicate that some motional averaging takes place at the Mn(II) site at room temperature. Unfortunately, the X-band spectra do not allow a

(35) De Vos, D. E.; Weckhuysen, B. M.; Bein, T. *J. Am. Chem. Soc.* **1996**, *118*, 9615−9622.

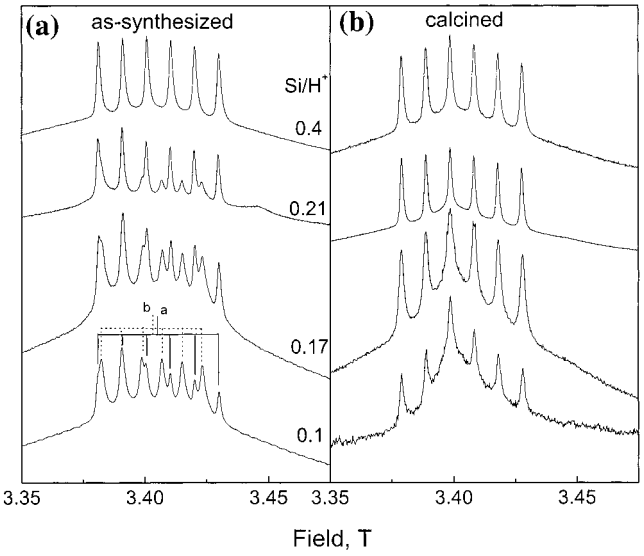

Figure 5. FS-ED EPR W-band spectra of MnMCM-41 prepared with different [Si]/[H^+] recorded at 4.5 K: (a) as-synthesized and (b) calcined. The ^{55}Mn hyperfine components of sites *a* and *b* are indicated on the figure.

straightforward determination of the ^{55}Mn hyperfine coupling without the application of spectral simulations.

In contrast to the X-band spectra, the W-band FS-ED EPR spectra, shown in Figure 5, are significantly simpler and highly resolved. The W-band FS-ED EPR spectrum of MnMCM-41, prepared with the [Si]/[H^+] = 0.4, shows a single well-resolved sextet with a splitting of 97 G and a *g*-value of 2.003, assigned to Mn(II) in site *a*. The spectra of the samples prepared with lower [Si]/[H^+], 0.1−0.21, exhibit two superimposed sextets, due to the existence of two types of Mn(II) centers (Figure 5a). The first has the same EPR parameters as site *a*, whereas the parameters of the second, referred to as site *b*, are $A = 82$ G, and $g = 2.014$. After calcination all samples exhibit a single, well-resolved sextet with $A = 97$ G, superimposed on a broad peak centered at $g \approx 2$. The relative intensity of the broad signal increases with [H^+] and it correlates with the relative amounts of site *b* in the as-synthesized materials, suggesting that it is associated with site *b*.

The EPR spectra of as-synthesized MnMCM-41 are highly sensitive to the water content of the sample. For example, the room temperature X-band spectrum of as-synthesized MnMCM-41 ([Si]/[H^+] = 0.1), which has not been completely dried (see Figure 6A), shows a well-resolved sextet without fine structure. Upon cooling to 150 K, each of the lines within the sextet exhibits a typical powder pattern characteristic of Mn(II) with a significant ZFS[23] (see Figure 6A,a). This indicates that the presence of excess water facilitates motional averaging at room temperature, which, in turn, reduces the contribution of the ZFS to the spectrum. Letting the sample dry for 2 weeks at room temperature yields a significantly broader signal (Figure 6A,b) due to the reduced mobility. The FS-ED W-band spectra of the dry and wet samples recorded at 4.5 K are presented in Figure 6B. The spectrum of the wet sample shows the presence of only one type of Mn(II) center with $A = 97$ G, similar to site *a*, whereas in the dry sample sites *a* and *b* coexist. These changes are reversible, namely, adding a few drops of water to the dried sample restores the narrower X-band EPR spectrum. The XRD patterns of the wet and dry samples are the same.

Mn(II) was also introduced into hydrothermally stable MCM-41 using the postsynthesis template-ion exchanged method.[17] This method was reported to introduce the Mn(II) into the silica

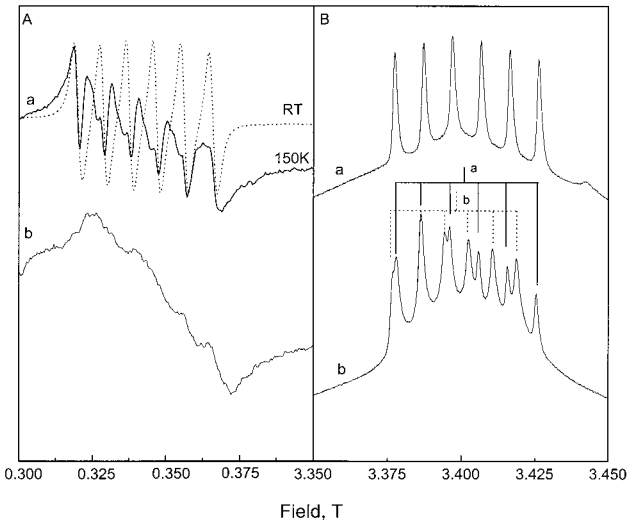

Figure 6. (A) X-band EPR spectra of (a) a wet sample of as-synthesized MnMCM-41 ([Si]/[H^+] = 0.1) recorded at 296 (dotted line) and 150 K (solid line) (b) after drying for 2 weeks at room temperature. (B) The corresponding FS-ED EPR W-band spectra (4.5 K) of the wet (a) and dry samples (b). The ^{55}Mn hyperfine components of sites *a* and *b* are indicated on the figure.

during the calcination process. The X-band spectrum of this sample exhibits the same sensitivity to water as as-synthesized MnMCM-41, and the FS-ED W-band spectrum of the calcined sample shows only one type of Mn(II), with the same hyperfine coupling constant as in site *a*.

(b) ENDOR Measurements. Further distinction between the two Mn(II) centers was obtained from ENDOR experiments that provide the hyperfine interaction of nearby nuclear spins coupled to Mn(II). Figure 7a shows the ^{1}H W-band Davies ENDOR spectrum of MnMCM-41 ([Si]/[H^+] = 0.4), which corresponds to site *a*. The spectrum was recorded at a magnetic field set to the high-field ^{55}Mn hyperfine component of the central EPR transitions, marked with **a** in the inset in Figure 7. At the field (∼3.4 T) and the low temperature (4.5 K) at which the experiments were performed, the intensities of the $|^1/_2, m\rangle \rightarrow |^3/_2, m\rangle$ and $|^3/_2, m\rangle \rightarrow |^5/_2, m\rangle$ EPR transitions are significantly diminished compared to the other transitions. Consequently, the ENDOR spectrum should exhibit signals arising primarily from the $M_S = -^5/_2, -^3/_2, -^1/_2, ^1/_2$ manifolds at

$$\nu(M_S) = |-\nu_I + M_S A| \qquad (1)$$

where ν_I is the nuclear Larmor frequency and *A* is the hyperfine coupling. For an axially symmetric tensor, the values of *A* at the canonical orientations, $\theta = 0, 90°$, are $A_{||}$ and $A_\perp$. These can be decomposed into an isotropic part, A_{iso}, and an anisotropic part, A_d, according to:

$$A_{||} = A_{iso} + 2A_d \qquad A_\perp = A_{iso} - A_d \qquad (2)$$

The ENDOR spectrum presented in Figure 7a exhibits several features centered about the ^{1}H Larmor frequency: a doublet with a splitting of 0.7 MHz, attributed to weakly coupled protons, and a powder pattern with $|A_{||}(^1\text{H})| = 7.1$ MHz and $|A_\perp(^1\text{H})| = 2.6$ MHz. The asymmetric appearance of the $A_{||}$ singularities is due to a superposition with the $-^3/_2 A_\perp$ singularity of the $M_S = -^3/_2$ manifold, originating from the $|-^3/_2, m\rangle \rightarrow |-^1/_2, m\rangle$ EPR transitions. Using eq 1 and the position of this signal the signs of $A_{||}(^1\text{H})$ and $A_\perp(^1\text{H})$ were determined, yielding $A_{iso} = 0.6 \pm 0.2$ MHz, $A_d = 3.2 \pm 0.2$ MHz. Applying the point-dipole approximation where $A_d = g_n\beta_n g\beta/hr^3$, a Mn(II)−H

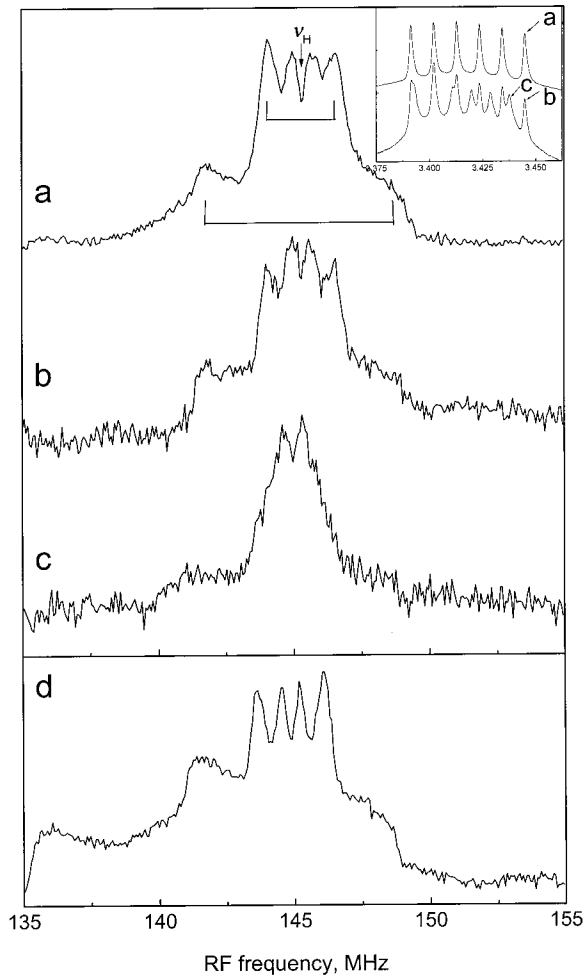

Figure 7. ^{1}H W-band Davies ENDOR spectra of (a) as-synthesized MnMCM-41 ([Si]/[H$^+$] = 0.4) recorded at a field position marked with **a** in the inset (3.413 T), (b) as-synthesized MnMCM-41 ([Si]/[H$^+$] = 0.17) recorded at position **b**, (c) same as (b) recorded at position **c** (3.406 T), and (d) calcined MnMCM-41 ([Si]/[H$^+$] = 0.17) recorded at position **a**. The doublets corresponding to the $A_\parallel$ and $A_\perp$ singularities of the water protons are indicated on the top spectrum.

distance of 2.9 Å is obtained, which is in good agreement with water ligand(s).[36−38]

ENDOR spectra of MnMCM-41 ([Si]/[H$^+$] = 0.17), which consists of both sites *a* and *b*, are shown in Figure 7b,c. The spectrum recorded at a field position selecting primarily a central transition of site *a* (Figure 7b) is similar to that of MnMCM-41 ([Si]/[H$^+$] = 0.4) (Figure 7a). In contrast, the spectrum measured at a field position set to a central transition of site *b* exhibits a doublet with a small coupling of 0.7 MHz (Figure 7c). The powder pattern typical of water coordination appears with very low intensity and is probably due to minor contributions from a $|-1/2, m\rangle \rightarrow |1/2, m\rangle$ transition of site *a* at this field. The ENDOR spectrum of calcined MnMCM-41 ([Si]/[H$^+$] = 0.17), depicted in Figure 7d, is similar to that of site *a* in the as-synthesized material, showing that the Mn(II) is coordinated to water. All samples, after calcination, independent of their [Si]/[H$^+$], showed the same ENDOR spectrum.

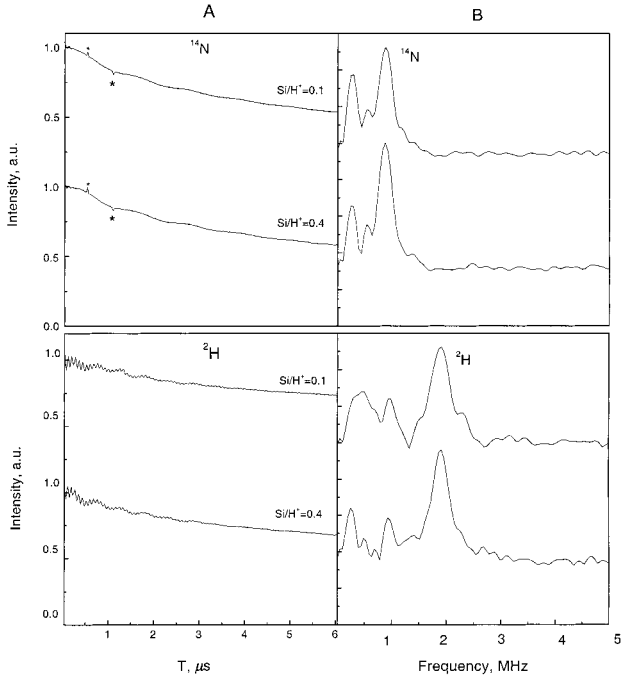

Figure 8. (A) X-band three-pulse ESEEM waveforms of as-synthesized MnMCM-41 ([Si]/[H$^+$] = 0.1) and MnMCM-41 ([Si]/[H$^+$] = 0.4) recorded at 4 K and B_0 = 0.3 T, corresponding to maximum echo intensity. The τ values were 0.541 and 0.23 μs optimized for ^{14}N and ^{2}H modulation, respectively. (B) The corresponding magnitude Fourier transforms. The asterisks in A indicate interferences from unwanted echoes that were not completely removed by the phase cycle.

(c) ESEEM Measurements. Using W-band ENDOR, it was possible to determine the state of water coordination of the Mn(II) in sites *a* and *b*. Additional information regarding the environment of the Mn(II) was obtained from X-band ESEEM experiments designed to probe its location with respect to the surfactant molecules. This was achieved by the modulation induced by the ^{14}N nucleus in the polar head of the surfactant molecules. The three-pulse ESEEM waveforms of MnMCM-41 ([Si]/[H$^+$] = 0.4), with Mn(II) in site *a* only, and of MnMCM-41 ([Si]/[H$^+$] = 0.1) ,where site *b* dominates, are depicted in Figure 8A. The corresponding FT-ESEEM spectra are shown in Figure 8B. The ^{14}N modulations are clear in both samples and the FT-ESEEM spectra show that the ^{14}N Larmor frequency peak is somewhat more intense in the sample consisting of only site *a*. Since the modulation depth is a function of the unpaired electron−nucleus distance and the number of nuclei around it,[30] this modulation depth difference indicates that in site *a* the Mn(II) is located closer to the polar head of surfactant molecules. The fact that ^{14}N modulation is observed at the Larmor frequency indicates that the ^{14}N quadrupole interaction is very small due to the symmetric (tetrahedral) environment of the nitrogen. ESEEM measurements were carried out also on samples synthesized with α-d_2CTAB ([Si]/[H$^+$] = 0.4 and 0.1). Both samples exhibit ^{2}H modulations (Figure 8) that are in agreement with the ^{14}N modulation experiments.

Discussion

In this section we first discuss the effect of [H$^+$] on the reaction kinetics and the properties of the MCM-41 product as determined from the XRD, NMR, and in situ EPR measurements. We then proceed with the description of the Mn(II) sites as determined from the various EPR/ENDOR techniques applied, and finally correlate the bulk properties of the final

(36) Tan, X.; Bernardo, M.; Thomann, H.; Scholes, C. P. *J. Chem. Phys.* **1993**, *98*, 5147−5157.
(37) Manikandan, P.; Carmieli, R.; Shane, T.; Calb (Gilboa), A. J.; Goldfarb, D. *J. Am. Chem. Soc.* **2000**, *122*, 3488−3494.
(38) Sham, T. K.; Hastings, J. M.; Perlman, M. L. *J. Am. Chem. Soc.* **1980**, *102*, 5904−5906.

product and the reaction kinetics with the factors that control the incorporation of the Mn(II) into the silica wall.

The final product of the $[Si]/[H^+] = 0.1$ gel mixture consists of a single hexagonal phase, phase A, with $d = 38$ Å. A decrease in $[H^+]$ results in the appearance of a second hexagonal phase, phase B, with $d = 43$ Å, and this phase becomes dominant at $[Si]/[H^+] = 0.4$. The ^{29}Si NMR spectra show that when $[Si]/[H^+] = 0.4$, the hydrolysis is relatively slow and silicate condensation, forming the silica wall, occurs prior to the completion of the TEOS hydrolysis. Under these conditions, organo-silica intermediates are trapped in the organic phase and act as "swelling" agents leading to the larger *d* spacing. The in situ EPR measurements showed that under these conditions the silicate condensation is considerably slower than for $[Si]/[H^+] = 0.1$. We therefore conclude that the increased acidity leads to a faster TEOS hydrolysis and silicate condensation. Hence, for $[Si]/[H^+] = 0.1$ a larger number of silicate species with the following decreasing acidity are present during the reaction:[39]

$$Si(OH)_4 < -Si-O-Si(OH)_3 < (-Si-O)_2Si(OH)_2 < (-Si-O)_3Si(OH)$$

The appearance of relatively large amounts of Q_2 and Q_3 in the NMR spectra shows that the degree of the silica condensation is incomplete for both $[Si]/[H^+] = 0.1$ and 0.4.

The application of high-field EPR/ENDOR has allowed us to distinguish between two types of Mn(II) centers in as-synthesized MnMCM-41, sites *a* and *b*. The relative amounts of the Mn(II) in the two sites depend on the $[Si^+]/[H^+]$ of the starting gel, where the final product of the $[Si]/[H^+] = 0.4$ gel mixture consists of site *a* only. The ^{55}Mn hyperfine coupling of 97 G and the ENDOR results show unambiguously that in this site the Mn(II) is in an octahedral symmetry and has water ligands. Furthermore, the Mn(II) is situated in the vicinity of template molecules as evident from the ^{14}N and ^{2}H modulations in the ESEEM traces. In addition, the X-band CW-EPR spectra recorded at room temperature and 150 K show that the Mn(II) center experiences some motional averaging which is facilitated by the presence of water. Since the Mn(II) cannot be washed away and it is situated in the vicinity of the surfactant molecules, it has to be anchored to the inner silica surface either through a silica oxygen ligand, as schematically represented in Figure 9, or by hydrogen bonds. The mobility induced by excess water is probably due to the softening effect of the water on the silica wall which in turn facilitates local motions of both the template molecules and the Mn(II) complex/ligands.

As the $[Si]/[H^+]$ of the reaction mixture decreases to 0.21, site *b* appears, and its relative amount increases with further increase of $[H^+]$. The characteristics of this site are significantly different from those of site *a*. It has a smaller ^{55}Mn hyperfine coupling, 82 G, and no water ligands, although the presence of one water or OH ligand cannot be ruled out due to the weak broad background in the ENDOR spectrum (see Figure 7). The Mn(II) in this site is also in the vicinity of the surfactant molecules, but somewhat further away than in site *a*. This, and the smaller ^{55}Mn hyperfine coupling, suggests that site *b* corresponds to Mn(II) in a tetrahedrally distorted site[40] situated within the silica wall, close to the internal surface. The properties of this site are highly sensitive to the water content of the sample. Adding a small amount of water (3 wt %) changes the hyperfine coupling to 97 G and induces significant local motions. This behavior suggests that the water causes hydroxylation of the surface releasing several coordination sites of the Mn(II) allowing them to coordinate water molecules, thereby reducing the local distortions, changing the hyperfine coupling and allowing water ligand rotation or exchange. A schematic illustration of this site and its response to water is depicted in Figure 9. Upon calcination, the spectral features characteristic of a well-dispersed site *b* disappear. It is not clear, however, if it is released from the silica wall and assumes the same properties as site *a* where it is anchored to the silica surface and coordinated to water molecules, or if it is responsible for the abroad unresolved spectrum that may represent Mn(II) centers with a large distribution of Hamiltonian parameters or small Mn(II) or Mn(IV) oxide clusters. The latter option is, however, less likely, as signals of clusters are usually hard to observe in pulsed experiments due to the fast echo decays.

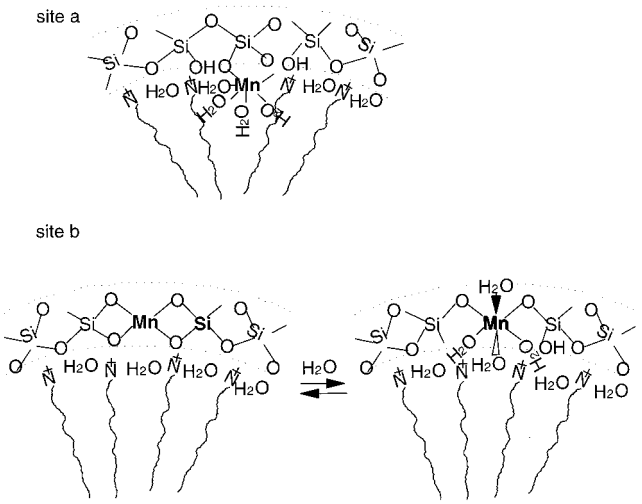

Figure 9. A schematic representation of the Mn(II) sites in MnMCM-41: (a) site *a* and (b) site *b* and its response to the water.

The possibility that site *b* is due to Mn(IV) rather than Mn(II) has been considered as well. Mn(IV) exhibits *g*-values less than 2.0, with hyperfine coupling values smaller than 72 G,[41] which are not too far from the parameters of site *b*. Assignment to Mn(IV) would imply that the reversible changes it undergoes upon water exposure involve oxidation/reduction according to the following: $Mn(IV) + H_2 \rightleftharpoons Mn(II) + {}^1/_2O_2 + 2H^+$. It is very unlikely that such a process takes place reversibly under very mild conditions. Moreover, MnMCM-41 was prepared under acidic conditions to avoid its oxidation to Mn(III) that occurs under basic conditions. It is therefore unlikely that the reduction in the pH, which prevents the oxidation of the Mn(II) to Mn(III), will generate Mn(IV).

Although the relative amount of Mn(II) in sites *a* and *b* seems to correlate with the different hexagonal phases A and B, it is improbable that the different pore size is responsible for the different Mn(II) properties. The formation of sites *a* and *b* is determined by the structural and surface characteristics of the silica wall and the degree of silicate condensations. Some of these properties also determine the relative amount of phase A or B, thereby explaining the above correlation. The Mn(II) can bind to one or more silicate species according to

$$Mn(H_2O)_6^{2+} + (-Si-O)_3Si(OH) \rightarrow Mn(H_2O)_5^{1+}[(-Si-O)_3SiO] + H_3O^+$$

(39) Iler, R. K. *The Chemistry of Silica Solubility, Polymerization, Colliod and Surface Properties, and Biochemistry*; John Wiley & Sons: New York, 1979; pp 172−304.

(40) Olender, Z.; Goldfarb, D.; Batista, J. *J. Am. Chem. Soc.* **1993**, *115*, 1106−1114.

(41) Kijlstra, W. S.; Poles, E. K.; Bliek, A. *J. Phys. Chem. B* **1997**, *101*, 309−316.

This process can continue until the Mn(II) loses most of its water ligands and becomes fully trapped in the silica wall with tetrahedral coordination, forming site *b*. Accordingly, the larger the concentration of silicate species, such as $(-Si-O)_3Si(OH)$, the higher is the probability to incorporate Mn(II) into the silica network. Hence, when the TEOS hydrolysis is incomplete, as for the reaction mixture with $[Si]/[H^+] = 0.1$, the probability for the formation of site *b* is reduced, hence site *a* predominates. Nevertheless, the above process is not highly favorable, since only 4% of the Mn(II) added to the synthesis gel remains in the final product.

X-band EPR and ESEEM studies on Mn-containing materials prepared under basic conditions showed that as-synthesized MnMCM-41 exhibits no EPR signal whereas after a calcination, hydration ,and dehydration, three Mn(II) species were observed.[13] Two were attributed to extraframework sites and the assignment of the third remains ambiguous, although it exhibits no hyperfine structure, possibly due to spin exchange. This indicates Mn(II) migration upon dehydration/hydration.[14]

Our results show that Mn(II) introduced into MCM-41 by the template-ion exchange method, followed by calcination, generates site *a*, and not site *b*, showing that Mn(II) ions are not incorporated into the bulk silica.

Conclusions

MnMCM-41 has been prepared under acidic conditions, and using high-field EPR/ENDOR it has been possible to distinguish two different Mn(II) sites, *a* and *b*, the relative amounts of which depend on the $[Si]/[H^+]$ in the reaction mixture. In site *a*, which predominates for gels with $[Si]/[H^+] = 0.4$, the Mn(II) is octahedrally coordinated by water ligands, and is anchored via one ligand position or hydrogen bonds to the channel surface. Site *b* has a distorted tetrahedral geometry and it predominates when $[Si]/[H^+] = 0.1$. It has no water ligands and is located within the silica close to the internal surface. In wet samples the addition of water "relaxes" the site, allows water coordination, and changes to octahedral symmetry. The formation of site *b* is favored under conditions of complete hydrolysis and faster silicate condensation which occurs at lower pH. Upon calcination the Mn(II) in site *b* is forced away from the silica and transforms into site *a*.

The application of high-field EPR and ENDOR offers unique new opportunities for characterizing Mn(II) sites in porous materials. Further combination with in situ EPR spectroscopy of spin probes and ^{29}Si MAS NMR spectroscopy provides insight into the incorporation mechanism that allows optimization and controls Mn(II) incorporation.

Acknowledgment. This work was supported by a grant from the Israeli Ministry of Science and Technology. We thank Dr. Tapas Sen for performing the ^{29}Si MAS NMR measurements. We are grateful to H. Zimmermann for providing the deuterated CTAB.

JA994165N